Available online www.jocpr.com

Journal of Chemical and Pharmaceutical Research, 2017, 9(8):1-7

Research Article

ISSN : 0975-7384
CODEN(USA) : JCPRC5

Synthesis and Characterization of Triethanolamine (TEA) Grafted Nano Sheets of Hydroxyapatite

Lokesh Kumar and Anupama Kaushik*

Department of Chemical Engineering and Technology, Panjab University, Chandigarh, India

---

ABSTRACT

The surface morphology of hydroxyapatite (HAp) was transformed into nano-sheets of rectangular shape by grafting the triethanolamine (TEA). The reaction was carried out using a precipitation method. The prepared HAp nano sheets were characterized using different techniques such as SEM, TEM, FTIR, XRD and WD-XRF in order to observe morphological, compositional and structural characteristics of newly formed HAp nano sheets. XRD analysis shows that the structure of HA remains almost unchanged with a slight effect on its crystallinity. The presence of TEA on to the HAp surface was also confirmed by the FTIR technique. SEM and TEM techniques depicted presence of TEA at HAp surface has significantly changed its overall morphology. The combined estimation of FTIR and WD-XRF studies however revealed a strong interaction between the grafted TEA molecules and surface groups of HAp. The grafting did not affect the pristine structure of HAp and stoichiometry of its Ca/P group. Further, the approximation of contact angle of HAp nano-sheets exhibited a strong hygroscopic tendency of this nano material.

Keywords: Hydroxyapatite; Triethanolamine; Scanning electron microscope; Transmission electron microscope; Contact angle

---

INTRODUCTION

Hydroxyapatite (HAp) has great potential to be successfully used as an adsorbents, catalyst and biomaterials such as for orthopedic implants [1]. It is derived from the various surfaces characteristics of HAp e.g. highly reactive functional groups at the surface, pH, acidity, high hydrophilic tendency and abundance of surface charges. Due to high surface reactivity of HAp, the material conducts the easy exchange of HPO4 2- groups by carbonate ions or organic substances [2]. Further, there are many other exclusive properties associated with the P-OH groups present at HAp surface that are responsible for the good adsorption of protein molecules and other organic species [3].

Since last decades, numerous research studies have been carried out using HAp especially with the aim to construct organic-mineral hybrid apatite system so as to get strong influence of these small organic species on the size and morphological properties of HAp [4-6]. As natural bone consists of inorganic/organic composite structure in the diameter about 20 nm and length about 50 nm [7], from the view point of bionics. Therefore, HAp/organic mineral constructs oriented research is of great importance now these days for composing a desired scaffold system with advanced features. In the frame work of HAp/organic mineral system research different processes have been proposed till date. Most of these based on the extent of interaction between Ca2+ or P ions and other anionic groups of organic minerals on the surface of HAp [8]. Different coupling agent have been used for this purpose such as organo functional silanes [9], dodecyl alcohol [10], photocrosslinkable chitosan [11], triethanolamine (TEA) [12], etidronic acid [13], hexyl, octyl, and decyl phosphate in mixed acetone/ water solvents [10] etc. These organic agents are highly beneficial for promotion of interfacial adhesion between filler and polymer matrix during scaffold

engineering. Nano-crystallized characteristics of HAp have proven to be of great biological importance [14]. For example, compared with conventionally crystallized HAp, nano-crystallized HAp can promote osteoblast adhesion and proliferation, osseointegration and deposition of calcium-containing minerals on its surface. Modification of surface of nano-hydroxyapatite is also possible and can yield very advance scaffold systems facilitating a speedy recovery of injured bones with high efficacy. Because of higher surface area, such a modified nano material can effectively improve hemocompatibility as well as load and stress-strain bearing characteristics (mechanical properties) of resultant scaffolds [15]. Thus, the much effort has been focused on development of nano-sized HAp powders with advance surface characteristics. The focus of this study is therefore mainly oriented around modification of surface of nano HAp using triethanolamine (TEA). An interesting fact about selection of TEA for this work is its salient nature to entrap the living cells and to facilitate their speedy growth which can be very useful in the bone tissue engineering [16]. Further, it provides nutritional supplements to the injured cells and efficiently removes toxic metals from the body. Moreover, it has capability of synthesis within a phosphate based network of HAp that proposes a pathway for the design of scaffold which is entirely degradable in an aqueous media such as biological fluids [17]. In this research paper, a precipitation technique was used for rendering TEA on the surface of HAp. The study reports production of highly reactive and biocompatible nano-sheets of HAp obtained in form of fine powder using the above methodology. The effect of grafting of TEA molecules on chemical, structural and morphological properties of the nano-HAp was investigated using different characterization techniques such as FTIR, XRD, WD-XRF, SEM and TEM etc.

MATERIALS AND METHOD

Materials

Calcium nitrate tetra hydrate ($CaNO_3.4H_2O$) (99%, AR) and Potassium dihydrogenphosphate (KH_2PO_4) (99%, AR) were procured from Merck India Ltd. Liquid Ammonia 25% concentration and triethanolamine (98%, AR) were purchased from Rankem India and CDH, respectively.

Synthesis of Nano Hydroxyapatite (HA)

HAp was synthesized according to a well-established sol gel method using calcium nitrate and potassium dihydrogenphosphate used as calcium and phosphorus precursors, respectively. Solution of calcium nitrate was added drop wise to a solution of potassium dihydrogenphosphate under stirring. The molar ratio of the Calcium nitrate and potassium dihydrogenphosphate was 1.67 and the pH was maintained at 10 using liquid ammonia. Gel obtained after precipitation was aged for 24 hrs and then centrifuged 3-4 times at 3000 RCF with double distilled water which was then dried overnight at 60°C in a vacuum oven. Finally the unmodified hydroxyapatite was sintered at different temperatures 400, 600 and 800°C in electrical furnace in air with heating rate of 10°C/min to obtain different particle size.

Grafting of TEA by a Co-precipitation Method

The surface of the above prepared sintered hydroxyapatite was modified by grafting the triethanolamine (TEA). TEA solution of 0.1M concentration in double distilled water was used for modification. 0.5 gm of prepared hydroxyapatite and 100 ml of 0.1 M TEA was mixed using mechanical stirring for 48 hrs at 25 ± 2°C temperature and pH was maintained using ammonia solution. Mixture so obtained was ultra-centrifuged 3-4 times at 6000 RCF in double distilled water for 10 minutes to remove the unreacted TEA and ammonia. The obtained composite material was dried in vacuum oven at 60°C for 24 hrs. Based on sintering temperature, samples were designated as TEA/HAp60, TEA/HAp400, TEA/HAp 600 and TEA/HAp800.

Characterization of Unmodified and Modified Hydroxyapatite Fourier transform infrared spectroscopy(FTIR):

The chemical structures of unmodified and modified hydroxyapatite were characterized by Fourier transform infrared spectroscopy (FT-IR) in Perkin Elmer RZX spectrometer using KBr technology. FTIR spectra were recorded in a spectral range of 4000–450 cm^{-1} with a resolution of 2 cm^{-1} with two scans for each sample.

X-ray diffraction:

Phase analysis was performed by X-ray diffractometer (XRD) using a Philips X'Pert Pro X-ray diffractometer system. The radiation was Cu Kα (λ = 0.15406 nm) with 40 kV voltage and 40 mA intensity. The mean crystallite

size (*D*) of the particles was calculated from the XRD line broadening measurement using the Scherrer equation [18], equation(1):

$$D = \frac{0.89\lambda}{\beta \cos\theta}, \quad (1)$$

Where λ is the wavelength (Cu-Kα), β is the full width at the half maximum of the HA (211) line and θ is the diffraction angle.

The fraction of crystalline phase (X_c) of the HA powders was evaluated by equation, (2)[19]:

$$X_c = \frac{1 - v_{112/300}}{I_{300}} \quad (2)$$

Where I_{300} is the intensity of (3 0 0) diffraction peak and $v_{112/300}$ is the intensity of the hollow between (1 1 2) and (3 0 0) diffraction peaks.

Transmission electron microscopy (TEM) and Scanning electron microscopy (SEM): The morphology of unmodified and modified hydroxyapatite was examined using transmission electron microscope (TEM) and Scanning Electron Microscope (SEM). TEM was also used to determine particle size. Model Hitachi-2100 was used for TEM and Images were taken at 80 kV accelerating voltage. A drop of a dilute sample in suspension was deposited on the carbon-coated grids and allowed to dry at room temperature. Particle size distribution of unmodified and modified hydroxyapatite in TEM images was undertaken using a UTHSCSA Image Tool image analyzer program (IT version 3). The images were loaded into the software and particle size measured using a two point measuring analysis. The scale of the software was calibrated using the scale bars on each TEM image (given below each TEM image). Approximately, 300 measurements were taken to obtain the distribution.

Contact angle measurement:

Contact angles of modified hydroxyapatite were measured on DSA 10 Mk 2 (Kruess) equipped with a video-imaging system. Sessile deionized-water drops were placed on the surface in the ambient environment, with a drop volume of 5 µL. Images were recorded after every 3 minutes and 5 images every second were taken with a video system. Contact angle values were calculated using the drop shape analysis system (DSA 1) and selected at 10 s.

Wavelength dispersive X-ray fluorescence (WD-XRF):

The elementary composition and Ca/P ratio of unmodified and modified hydroxyapatite was determined with Wavelength Dispersive X-ray Fluorescence-S8 Tiger from Bruker (WD-XRF), Germany.

RESULTS AND DISCUSSION

FTIR Analysis

FTIR spectra of unmodified and surface modified hydroxyapatite are shown in Figure 1. The presence of functional groups in all four TEA/mHA samples was also examined using Fourier transform infrared (FTIR) spectroscopy. All the TEA/HAp samples possess characteristic feature of triply degenerate asymmetric stretching mode of the P–O bond (ν3) in the apatite PO_4^{3-} group with the appearance of bands near 1100, 1050 and 1019 cm^{-1} in the FTIR spectra [20]. The bands at wave number 962 cm^{-1} attributes to the symmetric stretching mode of the P–O bond (ν1). Additional bands near regions of low wave numbers i.e. 602, 571 and 560 cm^{-1} represent the bending modes of the O–P–O bond (ν4) [21]. The peaks observed in the region between 3567 and 3571 cm^{-1} and the weak band at 633 cm^{-1} can, respectively, are attributed to the stretching (νs) and vibration modes (νL) of the structural hydroxyl anions in HAp samples [22]. The obtained spectra of the TEA/HAp samples also depict two weak peaks near region 2860 and 2970 cm^{-1} which are attribute to characteristic feature of -CH_2 group and ensures presence of TEA in the dried HAp samples. FTIR spectra also depicts characteristic peaks for hydroxyl group in all the five samples positioned at 3561, 3565, 3570, and 3571 cm^{-1} [23]. The important information obtained from these FTIR spectra is observance of blue-shifting in position of peaks of hydroxyl group with respect to standard FTIR absorption value (3570 cm^{-1}) in all TEA/HAp samples [24]. The observed shift may have originated from the hydrogen bonds between -OH group in TEA and O–H at the surface of HAp nano crystals. This shift, in combination with the progressive enhancement of -

OH stretching mode (at 3571 cm^{-1}) and vibration mode (at 633 cm^{-1}) indicates the disappearance of the interaction between the HAp nanocrystals and TEA. In other words, TEA desorbs slowly from the surface of HAp nanoparticles into water owing to unstable surface adsorption due to increase in sintering temperature [25]. The appearance of twin peaks at wave number 1411 and 1460 cm^{-1} and the single peak at 877 cm^{-1} in the present spectra suggests the presence of A-type (when CO_3^{2-} is substituted for OH-) and B-type (when CO_3^{2-} is substituted for PO_4^{3-}) carbonate ion substitutions in the TEA/HAp samples [23]. The required CO_3^{-2} ions for these substitutions might have come from CO_3^{-2} impurities in the reactants and/or from dissolved atmospheric CO_2.

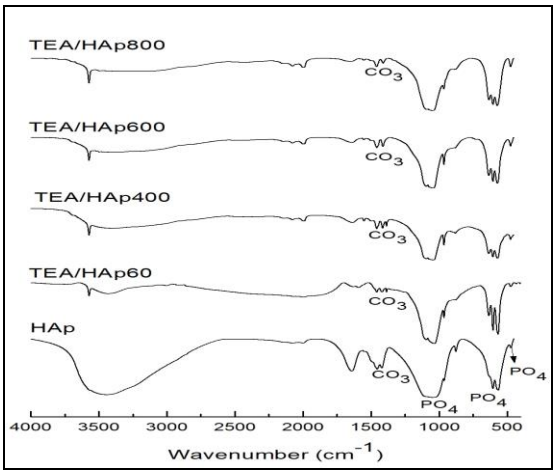

Figure 1: FTIR Spectra of unmodified and modified Hap by grafting of TEA

XRD Analysis

Figure 2 shows the XRD pattern of unmodified and modified HAp. The amounts of crystallinity and crystallite size calculated (using Scherrer equation) from XRD pattern of samples TEA/HAp60, TEA/HAp400 and TEA/HAp800 have been given in Table 1. The characteristic peaks of modified HAp are shown at 2θ = 26°, 32°, 33°, 34° and 40°, 49°, 53° that correspond to (002), (211), (300), (202), (310), (213) and (004) plane [20]. The results clearly depict increase in crystallite size as well as crystallinity with the increase in sintering temperature. XRD patterns of TEA/HAp800 shows no traces of secondary phases that directly indicate high purity in the final product [25]. WDXRF analysis (Table 1) for this TEA/HAp800 sample exhibited calcium and phosphorus ratio (Ca/P) of 1.64 ± 0.06 which is in proximity with the desired value of 1.67(Ca/P) [26].

Morphological Analysis

TEM micrographs for TEA/HAp samples have also been shown in Figure 3 at room temperature. From Figure 3e, it is depicted that pure HAp are individual particles with irregular rod like shapes. When the HAp particles are modified with TEA, the particle morphology steadily changes from rod like to sheet type with increase in particle size. The prepared sample consists of sheet like morphology with size in the range of 14-18 nm. With increase in the temperature to 400°C, TEA/HAp400 particles retained the similar morphology but their size has increased and observed to be within the range between 20-30 nm. At sintering temperature 400°C, significant variation in the morphology of the sheet-shaped HAp particles was reported (Figure 3c) in addition with the increase in size of the particles. The size of nano particles was observed to be in the range between 25-40 nm. At the final sintering temperature i.e. 800°C, the TEA/mHAp800 particles exhibited only spherical morphology with further increased diameter in the range of 70-90 nm. Suge et al. [27] has also observed similar morphological changes for HAp samples with the increase in reaction temperature. This indicates an effective interaction of molecules of TEA with surface groups of the HAp nano crystals during high temperature sintering that in turn facilitated the growth of HAp nano particles. Thus, the obtained TEM micrographs of the TEA/mHAp samples clearly shows occurrence of a temperature driven phenomena that varies degree of interaction between TEA molecule and HAp nano crystal resulting in overall change in surface morphology of the HAp nano particles [20]. FTIR analysis has also confirmed the sintering temperature driven interaction between TEA molecules and HAp nano particle. The analysis further indicate occurrence of some special properties as a result of TEA/HAp interaction that can be highly significant

during scaffold application. For example, such a modifications on the surface of these biomaterial can be an effective technique to further enhance the biocompatibility which significantly improves and accelerate invasion of bone tissues in scaffolds.

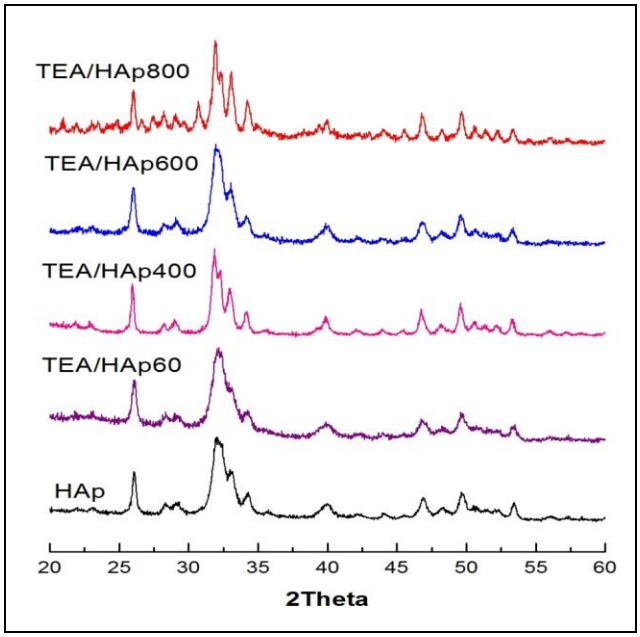

Figure2: XRD profiles of unmodified and modified Hap by grafting of TEA

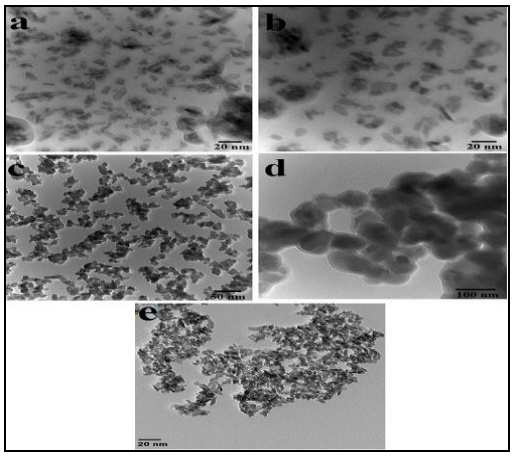

Figure 3: TEM Images of (a) TEA/HAp60, (b) TEA/HAp400, (c) TEA/HAp600, (d) TEA/HAp800 and (e) HAp

SEM micrographs shown in Figure 4 depict morphology of TEA/mHAp samples and are in consistent with that obtained from the TEM analysis. The SEM images of TEA/mHAp60 sample exhibited irregular sheet like shape and this morphology further changed in shape and size that increased from 10 to 90 nm when sintering temperature increased from 60 to 800°C. Increasing surface interactions of individual HAp nano particles with molecules of TEA possibly resulted in promotion of the formation of layered particles. The SEM images further reported reduction in agglomeration of the particles with the sintering temperature. Best results were obtained for sample TEA/HAp400 as it shows sheet morphology of HAp resembling the structure of bone. Hence, such a characteristic ensures a better biocompatibility of TEA/HAp nano particles in tissue engineering. Further, results indicates a significant improvement in mechanical strength due to its high specific surface area, superior and defect free chemical structure and improved resemblance with the human bone due to its modification at micro level [28].

Crystallite size as estimated from XRD results are in the same order of magnitude suggesting that the particle size increased with increase in sintering temperature [12].

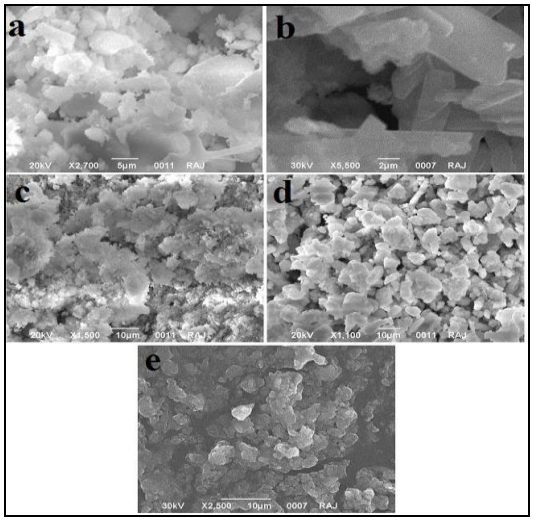

Figure 4: SEM Images of (a) TEA/HAp60, (b) TEA/HAp400, (c) TEA/HAp600, (d) TEA/HAp800 and (e) HAp

Contact Angle Analysis

The contact angles of modified Hydroxyapatite (HAp) are shown in Figure 5. Contact angle characterizes the wettability of the surface of a solid by a liquid i.e. the interaction between a solid and a liquid surface at the interface. Increased wettability enhances interaction between implant surfaces and the biologic environment during osseointegration. [29]. After surface modification no critical contrasts were showed in contact angles which were below 40° revealing the super hydrophilic behavior, showing that the contact angles were independent of surface modification.

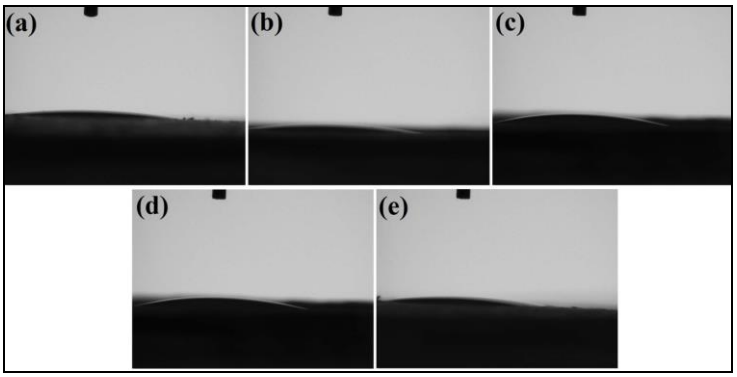

Figure 5: Contact Angle images of (a) TEA/HAp60, (b) TEA/HAp400, (c) TEA/HAp600, (d) TEA/HAp800 and (e) HAp

WD-XRF Analysis

The chemical composition, Ca/P ratio and percent carbon of unmodified and modified HAp sintered at different temperature determined using WD-XRF (Wavelength Dispersive X-ray Fluorescence) are given in Table 1. From the data in the Table 1 it is clear that TEA did not significantly affect the stoichiometry of HAp and the Ca/P molar ratio for modified HAp is close to the stoichiometry value of 1.67 ± 0.02 [26]. The incorporation of TEA in HAp structure is also confirmed by the total carbon analysis, showing almost constant amount of the total carbon ~0.90% in the powder while the total amount of carbon in unmodified HAp is less than 0.30.

Table 1: Crystallite size, crystallinity, Ca/P ratio and total % carbon of unmodified and modified Hap

Sample ID	Sintering Temperature (°C)	Crystallite size (nm)	Crystallinity (%)	Ca/P ratio	Total %C
HAp	**60**	~10	39	1.65	0.2
TEA/HAp60	**60**	~12	40	1.66	0.9
TEA/HAp 400	**400**	~43	59	1.67	0.89
TEA/HAp 600	**600**	~72	80	1.71	0.86
TEA/HAp 800	**800**	~92	90	1.72	0.85

CONCLUSION

The overall purpose of the study was to modification of HAp nanoparticles using TEA. Modification of HAp was successfully done by grafting of TEA on the surface of HAp as observed in XRD and FTIR results. The chemical compositions and structural study showed undisturbed stoichiometry and phase stability of surface modified HAp which is a good indication. Further, morphology and particle size studied using SEM and TEM technique confirmed improvement in agglomeration tendency, crystallite size and shape of HAp nano particles. The study revealed that TEA/HAp400 sample modified at 400°C showed sheet type shape with high agglomeration tendency and can be best used in tissue engineering. The surface modifying agent used in this study can act as an interface providing a strong bond between HAp and polymer matrices that can possibly improve bioactivity of scaffolds in bone tissue engineering.

REFERENCES

[1] XF Qian; T Kamegawa; K Mori; HX Li; H Yamashita. *J Phys Chem C*. **2013**. 117(38), 19544-19551.
[2] M Corno; A Rimola; V Bolis; P Ugliengo. *Physical Chemistry Chemical Physics*. **2010,** 12(24), 6309-6329.
[3] JR Long; WJ Shaw; PS Stayton; GP Drobny. *Biochemistry*. **2001**, 40(51), 15451-15455.
[4] HW Choi; HJ Lee; KJ Kim; HM Kim; SC Lee. *J Colloid Interface Sci*. **2006**, 304(1), 277-281.
[5] X Qiu; Z Hong; J Hu; L Chen; X Chen; X Jing. *Biomacromolecules*. **2005**, 6(3), 1193-1199.
[6] Z Opre; D Ferri; F Krumeich; T Mallat; A Baiker. *J Catalysis.* **2006**, 241(2), 287-295.
[7] J Li; Y Chen; Y Yin; F Yao; K Yao. *Biomaterials*. **2007,** 28(5), 781-790.
[8] F Wang; B Cao; C Mao. *Chem Mater.* **2010**, 22(12), 3630-3636.
[9] V Cauda; A Schlossbauer; T Bein. *Microporous and Mesoporous Materials*. **2010**, 132(1), 60-71.
[10] L Borum-Nicholas; OC Wilson. *Biomaterials.* **2003**, 24(21), 3671-3679.
[11] IY Kim; SJ Seo; HS Moon; MK Yoo; IY Park; BC Kim; CS Cho. *Biotechnology Advances*. **2008**, 26(1), 1-21.
[12] F Mohandes; M Salavati-Niasari. *Materials Science and Engineering: C*. **2014**, 40, 288-298.
[13] M Othmani; A Aissa; CG Bac; F Rachdi; M Debbabi. *Applied Surface Science*. **2013** 274, 151-157.
[14] S Rahavi; O Ghaderi; A Monshi; MH Fathi. *Russian J Non-Ferrous Metals*. **2017,** 58(3), 276-286.
[15] D Kai; SS Liow; XJ Loh, *Materials Sci Engg*: C. **2014,** 45, 659-670.
[16] JJ Valdes; ER Valdes. National Defense Univ Washington Dc Center For Technology And National Security Policy. **2010**.
[17] M Colilla; M Manzano; I Izquierdo-Barba; M Vallet-Regí; C Boissiere; CN Sanchez. *Chem Materials*. **2009**, 22(5), 1821-1830.
[18] A Monshi; MR Foroughi; MR Monshi. *World J Nano Sci Engg*. **2012,** 2(3), 154-160.
[19] SE Ahn; JS Lee; H Kim; S Kim; BH Kang; KH Kim; GT Kim. *Appl Phys Letters*. **2004,** 84(24), 5022-5024.
[20] N Puvvada; PK Panigrahi; H Kalita; KR Chakraborty; A Pathak. *Applied Nanosci*. **2013**, 3(3), 203-209.
[21] N Patel; SM Best; W Bonfield; IR Gibson; KA Hing; E Damien; PA Revell. *J Mat Sci: Mat Med*. **2002**, 13(12), 1199-1206.
[22] JM Oliveira; MT Rodrigues; SS Silva; PB Malafaya; ME Gomes; CA Viegas; IR Dias; JT Azevedo; JF Mano; RL Reis. *Biomaterials.* **2006**, 27(36), 6123-6137.
[23] IR Gibson; W Bonfield. *J Biomed Mat Res Part A.* **2002,** 59(4), 697-708.
[24] MP Da Silva; JH Lima; GA Soares; CN Elias; MC De Andrade; SM Best; IR Gibson. *Surface and Coatings Tech*. **2001**, 137(2), 270-276.
[25] RN Panda; MF Hsieh; RJ Chung; TS Chin. *J Phys Chem Solids.* **2003,** 64(2), 193-199.
[26] AA Shaltout, MM Gomma, MW Ali Bik. *X Ray Spectrometry*. **2012**, 41(6), 355-362.
[27] T Suge; K Ishikawa; A Kawasaki; M Yoshiyama; K Asaoka; S Ebisu. *J Dental Res.* **1995**, 74(10), 1709-1714.
[28] H Zhou; J Lee. *Acta biomaterialia*. **2011**, 7(7), 2769-2781.
[29] N Eliaz; S Shmueli; I Shur; D Benayahu; D Aronov; G Rosenman. *Acta biomaterialia*. **2009,** 5(8), 3178-3191.